Electronic structure of the diamond crystal based on an improved cellular calculation

J. R. Leite,* B. I. Bennett, and F. Herman
IBM Research Laboratory, San Jose, California 95193
(Received 8 January 1975)

The band structure of diamond has been determined using Slater's cellular method. Calculations were carried out with the unit cell partitioned into two and then four space-filling polyhedra. The dependence of the energy-level structure on the choice of matching points and cellular basis functions is carefully examined. Once a sufficient number of cellular basis functions (tetrahedral harmonics) is introduced, the precise arrangement of the matching points is no longer critical, and substantially the same energy-level structure is obtained for a wide variety of matching-point configurations. Tetrahedral harmonic expansions including $l_{max} = 12$ are sufficient to ensure reasonable convergence at the zone points Γ, X, and L. Some energy levels converge with $l_{max} \geq 8$. Most early attempts to calculate the band structure of diamond-type crystals using the cellular method were quantitatively unsatisfactory because too few basis functions were used. The present cellular results based on fourfold partitioning compare favorably with orthogonalized-plane-wave (OPW) results and with experiment. The lowest conduction-band level at the zone center is found to be Γ_{15} in agreement with OPW calculations but in disagreement with recent nonlocal-empirical-pseudopotential calculations.

I. INTRODUCTION

One of the earliest attempts to solve the crystal wave equation for a realistic crystal model was that of Wigner and Seitz.[1] In their classic study of metallic sodium, the crystal volume was first decomposed into space-filling atomic polyhedra (Wigner-Seitz cells), then these polyhedra were replaced by equivalent volume spheres, and finally suitable boundary conditions were imposed on the surfaces of these spheres. By reducing the crystal wave equation to a central-field problem in each of these spheres, it was possible to make considerable progress in understanding the electronic properties of metallic sodium.

An improved cellular method was suggested by Slater[2] shortly thereafter. In Slater's scheme, the atomic polyhedra are retained, and the boundary conditions are imposed on the surfaces of these polyhedra. Slater's cellular method has been applied in various forms to diamond[3-5] and silicon.[6-9] In his pioneering study of the band structure of diamond, Kimball[3] imposed the boundary conditions only at the centers of the hexagonal faces of the atomic polyhedra (Kimball points). Similar studies of diamond were carried out at about the same time by Hund and Mrowka.[4] Later, Zehler[5] studied diamond by imposing the boundary conditions on circles lying on the hexagonal faces of the atomic polyhedra. These circles—the so-called von der Lage and Bethe[10] circles—represent the intersection of neighboring equivalent volume spheres.

In a 1953 study of silicon, Yamaka and Sugita[8] imposed boundary conditions both at the Kimball points and on the von der Lage and Bethe circles. This and earlier cellular calculations of diamond-type crystals were of considerable qualitative interest. However, they were quantitatively unreliable. The first quantitatively successful calculation of the band structure of diamond (which pointed to the many-valley conduction-band structure) was that of Herman[11] using the orthogonalized-plane-wave (OPW) method. Later theoretical and experimental studies of the band structure of diamond have been reviewed by Herman, Kortum, and Kuglin,[12] and more extensively by Buberman.[13]

In the earliest cellular calculations for silicon[7,8] based on isolated point matching, it was found that the calculated energy levels depended on the choice of matching points (and on the related choice of cellular basis functions). This apparent lack of convergence prompted subsequent investigators[9] to satisfy the boundary conditions in a least-squares sense over a large number of points spanning all the polyhedral faces, rather than at a limited number of points. This development stemmed from Kohn's[14] demonstration that Slater's cellular method could be derived from a variational principle. (Zehler[5] had also studied diamond from this point of view.) Altmann and his collaborators[15] have carried the variational cellular method further than most, obtaining satisfactory solutions for many metallic crystals. Ziman[16] has recently reviewed the cellular method and its relationship to other band-structure methods.

During the past few years, the energy-band structure of diamond has been investigated by a variety of methods, including the OPW method,[12,17] the empirical-pseudopotential method (EPM),[18-20] the augmented-plane-wave (APW) method,[21] the linear-combination-of-atomic-orbitals (LCAO) method,[22] and the discrete variational method (DVM).[23,24] There have also been extensive ex-

perimental studies during this period, particularly optical[25-27] and x-ray photoemission[28] measurements. In spite of all this progress, there is still considerable controversy[12,18-24] regarding the detailed structure of the conduction bands, including the assignment of the lowest conduction-band level at Γ. Is it Γ_{15} or Γ_2,?

The purpose of the present study is twofold: First, to understand the reason why many early investigators[3-9] obtained disappointing results for diamond using the cellular method, and second, to obtain better results for the band structure of diamond using an improved version of the cellular method.

The paper is organized as follows: In Sec. II, we review the essential features of the cellular method as it applies to the diamond structure. In Sec. III we indicate how the unit cell of diamond can be partitioned into two atomic cells, as in the work of Kimball,[3] or into two atomic plus two interstitial cells, as in more recent work by Keller[29] and Williams and Morgan.[30] In Sec. IV, we discuss the construction of the cellular potentials. The simplest cellular solutions for diamond based on twofold and fourfold partitioning of the unit cell are reported in Secs. V and VI, and improved solutions in Secs. VII and VIII. Considerable emphasis is placed on understanding the relationship between the calculated energy-level structure and the choice of basis functions and matching points.

II. CELLULAR METHOD APPLIED TO THE DIAMOND STRUCTURE

The theoretical basis of the cellular method has been discussed by many authors (see, for example, Refs. 2, 14, and 16). In order to establish our notation, we will review the theory briefly, indicating how it can be applied to the diamond structure. According to the cellular method of Slater,[2] a crystal is decomposed into space-filling atomic polyhedra (Wigner-Seitz cells), one surrounding each lattice site A. By construction, all points in polyhedron A lie closer to lattice site A than to any other lattice site. Depending on the choice of lattice site, we can construct atomic or interstitial polyhedra.

In the simplest form of the cellular method, the crystal potential is approximated within each polyhedron by its spherical average with respect to the center of the polyhedron. In this paper we will confine our attention to spherical cellular potentials. The crystal wave function is expanded in spherical harmonics in each polyhedron; for example, in polyhedron A, the cellular wave function corresponding to energy eigenvalue E would be written as follows:

$$\psi^E(\vec{r}_A) = \sum_{l,m} C_{l,m}^{E,A} R_l^E(r_A) Y_{l,m}(\theta_A, \phi_A), \tag{1}$$

where $\vec{r}_A = (r_A, \theta_A, \phi_A)$ is a radius vector with origin at site A, the $Y_{l,m}(\theta_A, \phi_A)$ are normalized spherical harmonics, the $R_l^E(r_A)$ are the solutions of the radial Schrödinger equation (for energy E), and the $C_{l,m}^{E,A}$ are undetermined expansion coefficients.

The boundary conditions relating the crystal wave function and its normal derivative in different polyhedra A and B may be stated as follows:

$$\psi^E(\vec{r})\big|_{\vec{r}=\vec{r}_A} = e^{i\vec{k}\cdot\vec{R}} \psi^E(\vec{r})\big|_{\vec{r}=\vec{r}_B}, \tag{2}$$

$$\hat{n}_A \cdot \nabla\psi^E(\vec{r})\big|_{\vec{r}=\vec{r}_A} = -e^{i\vec{k}\cdot\vec{R}} \hat{n}_B \cdot \nabla\psi^E(\vec{r})\big|_{\vec{r}=\vec{r}_B}, \tag{3}$$

where the points $\vec{r}_A$ and $\vec{r}_B$, which lie on the surfaces of polyhedra A and B, are separated by a direct lattice vector $\vec{R}$. The outward-pointing normal is always represented by $\hat{n}$ (cf. Fig. 1). If $\vec{R} = (0, 0, 0)$, Eqs. (2) and (3) ensure the continuity of the crystal wave function and its normal derivative on the surface common to polyhedra A and B. Otherwise, these equations express the crystal periodicity (Bloch) conditions appropriate to reduced wave vector $\vec{k}$. For a fixed value of $\vec{k}$, there will be a set of eigensolutions corresponding to different energy bands. For a fixed value of E, there will be a family of solutions for different values of $\vec{k}$ if E lies in an allowed band. These map out a constant energy surface in the reduced zone. If E falls in a forbidden band, there will be no solutions (with real $\vec{k}$). Thus, Eqs. (2) and (3) lead to the dispersion relations connecting E and $\vec{k}$.

In principle, one should impose boundary conditions on the surfaces of all the polyhedra into which the unit cell is decomposed. This is in fact done in the variational version of the cellular method.[9,14] For our purposes, however, it will be sufficient to consider a limited set of matching points suitably arranged on the various polyhedral surfaces, and a corresponding number of spherical harmonics suitably distributed among the

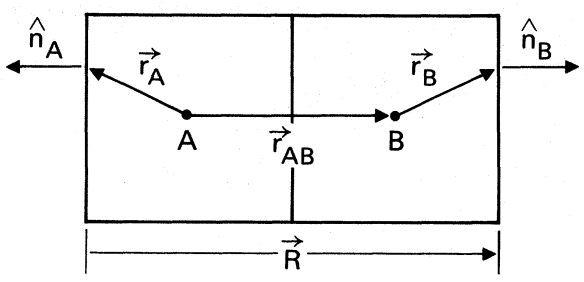

FIG. 1. Notation for cellular boundary conditions.

various polyhedra in the unit cell. If the total number of matching points is N ($N/2$ pairs of geometrically distinct points), and the total number of spherical harmonics (all polyhedra) is N, Eqs. (2) and (3) each define $N/2$ linear equations, making a total of N linear equations in all.

For all the boundary conditions expressed by Eqs. (2) and (3) to be satisfied nontrivially, the corresponding $N \times N$ determinant must vanish. This will occur for certain values of E, which are the energy eigenvalues. Thus, one evaluates the radial wave functions and their normal derivatives as a function of E at all required matching points, and with this information in hand searches for the zeros of the determinant as a function of E. Having thereby established the energy eigenvalues one can calculate the corresponding eigenvector components, i.e., the C coefficients. In the present study we concentrated on the eigenvalues, and paid only slight attention to the eigenvectors.

To recapitulate, we will satisfy the boundary conditions at a limited number of matching points. Our primary interest will be the relationship between the choice of matching points and the calculated energy-level structure.

III. DECOMPOSITION OF THE UNIT CELL INTO SUBCELLS

According to the more usual representation of a diamond crystal (two interpenetrating fcc carbon lattices), there are two atomic polyhedra per unit cell. Each of these has the tetrahedrally symmetric form indicated in Fig. 2. This representation was used by Kimball[3] and by most subsequent investigators. The principal advantage is simplicity. The principal disadvantage is the aspherical shape. To dramatize this aspect, we note that the ratio of the distances from the nucleus to the furthest and the nearest points on the boundary is 3. It is most unlikely that the crystal potential can be approximated satisfactorily by its spherical average in the outer reaches of this atomic polyhedron (capped tetrahedron). The spherical approximation for the cellular potential becomes progressively worse as we move outside the inscribed sphere toward the caps. Fully $\frac{2}{3}$ of the volume of the atomic polyhedron lies outside the inscribed sphere.

An alternate representation[29,30] treats the diamond structure as two interpenetrating diamond lattices, one of which locates the atomic positions, and the other, the interstitial positions. If one

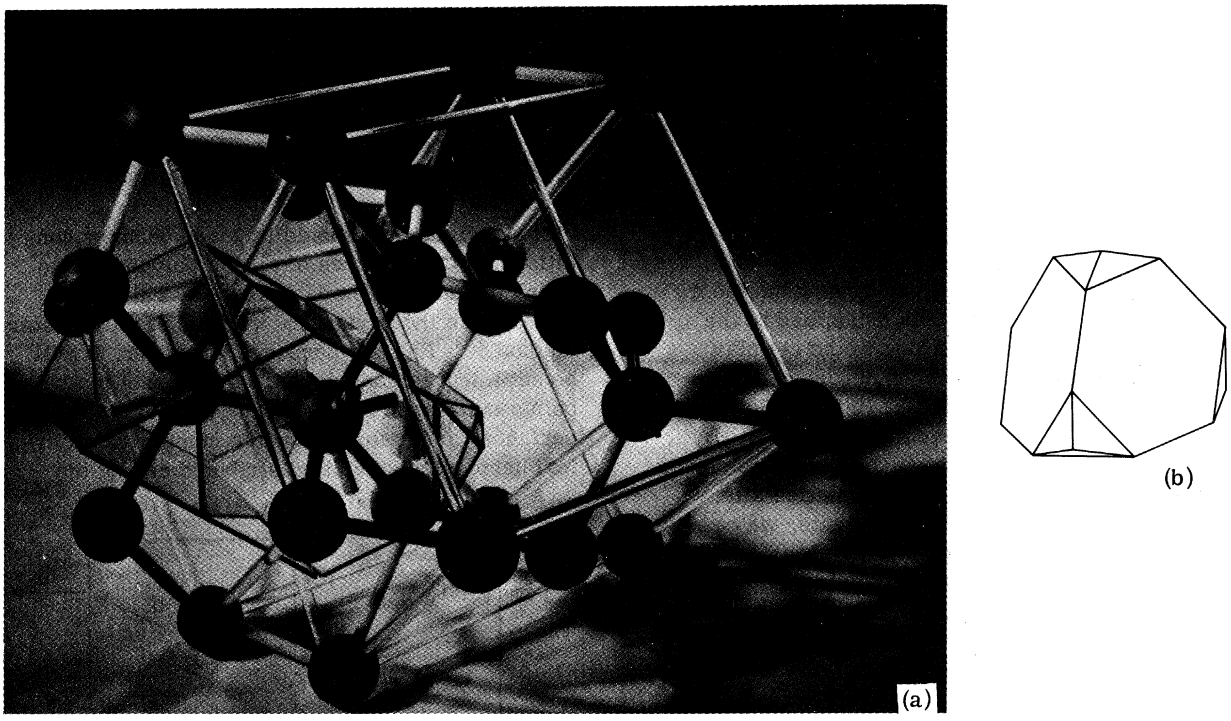

FIG. 2. (a) Model of diamond lattice showing the two Wigner-Seitz atomic polyhedra which together form the unit cell. All the hexagonal faces and only a few of the triangular faces of the atomic polyhedra are shown. The transparent rods indicate two interpenetrating unit cubes. The unit cube edge is a_L. (b) Atomic polyhedron for diamond structure (twofold partitioning of unit cell).

ignores the nature of these positions, and treats them all alike, then one has a body-centered cubic lattice, for which the Wigner-Seitz polyhedron is a truncated octahedron. It is convenient to define the unit cell as a string of four such truncated octahedra, as indicated in Fig. 3. We will place the carbon sites at (0, 0, 0) and $a_L(\frac{1}{4}, \frac{1}{4}, \frac{1}{4})$, and the interstitial sites at $a_L(\frac{2}{4}, \frac{2}{4}, \frac{2}{4})$ and $a_L(\frac{3}{4}, \frac{3}{4}, \frac{3}{4})$, where a_L is the unit cube edge. The truncated octahedra of Fig. 3 are considerably closer to spheres than are the capped tetrahedra of Fig. 2. The ratio of the distances from the center of the truncated octahedron to the furthest and nearest points on the surface is $(\frac{5}{3})^{1/2} = 1.29$ (which is to be compared with the ratio of 3 for the capped tetrahedron).

Because of the smaller size and more spherical shape of the atomic and interstitial polyhedra of Fig. 3, relative to the atomic polyhedra of Fig. 2, it is reasonable to expect a spherical average of the crystal potential to be a better approximation in the former than in the latter. Offsetting this advantage is the increase in the number of polyhedra that have to be taken into account. Although the polyhedra in Fig. 3 are octahedral in the form, the reader should bear in mind that the site symmetry is still tetrahedral (T_d) at all atomic and interstitial sites in this representation.

Of course, different numbers of spherical harmonics could be introduced in the atomic and interstitial polyhedra. However, we find it convenient to use the same number of spherical harmonics in both types of polyhedra.

In the present work we will carry out most of our studies using first the twofold and then the fourfold decomposition of the unit cell. This will give us some insight into the relative merits of these two representations.

IV. CONSTRUCTION OF CELLULAR POTENTIALS

The crystal potential can be expressed as the sum of a Coulomb term and an exchange term. The crystal Coulomb potential was represented by a spatial superposition of atomic Coulomb potentials, one centered at each atomic site. The spherical average of the crystal Coulomb potential was then obtained for the tetrahedral cell of Fig. 2, and for the octahedral atomic and interstitial cells of Fig. 3. This involved averaging the contributions of all neighboring atoms which made significant contributions to the sum throughout the cellular regions. The atomic potentials themselves were obtained from self-consistent Hartree-Fock-Slater atomic calculations with the statistical exchange parameter set equal to unity.[31]

The crystal charge density was obtained by forming an analogous spatial superposition of free-atom charge densities. Within each atomic or interstitial cell, the spherical average of the cube root of the crystal charge density was calculated, and this quantity was used to determine the spherically averaged Slater-type statistical exchange potential.

Spherically averaged cellular crystal potentials (Coulomb plus exchange) were obtained in this way using as many as 16 shells of neighboring atoms. Once the nearest six shells were taken into account, the inclusion of additional shells of atoms had a negligible effect on the calculated cellular potentials. The method used here for constructing crystal potentials is similar but not identical to that used by Rudge[17] in a recent unpublished OPW band calculation and in many earlier OPW band calculations for semiconductors and insulators.[32-35]

The crystal potential used in the present studies differs in two significant respects from that used in the OPW band calculations just cited.[17,32-35]

(a) In the present work, the cellular exchange

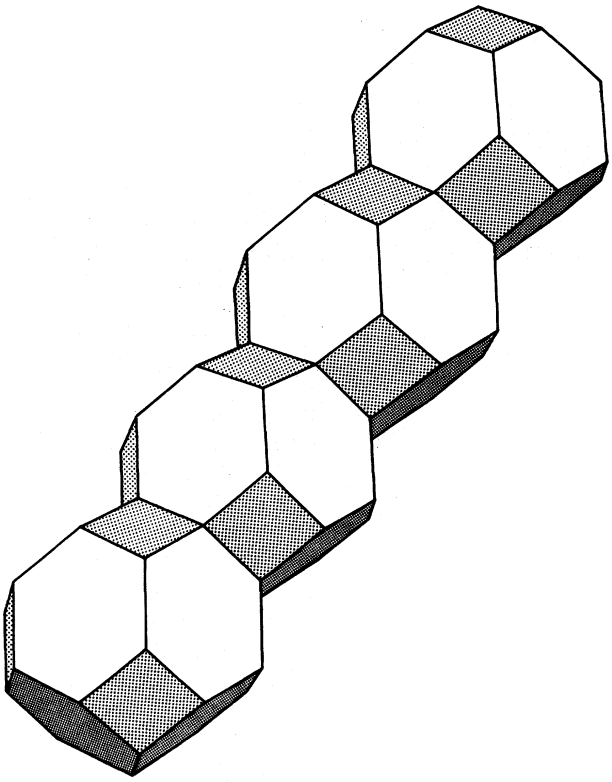

FIG. 3. Unit cell of diamond structure as represented by four truncated octahedra strung out along the unit cube diagonal. The lower two are atomic polyhedra and the upper two are interstitial polyhedra (fourfold partitioning of unit cell).

potential is taken as proportional to the cube root of the sum of the superimposed atomic charge densities, while in the other work the sum of the cube roots of atomic charge densities is used. The latter choice is equivalent to a superposition of atomic exchange potentials. While the present approach is closer to the letter of the statistical exchange approximation, in practice the cube root of the sum and the sum of the cube roots of strongly overlapping atomic charge densities leads to nearly the same crystal exchange potential, as demonstrated for silicon and germanium in earlier calculations.[35] The differences between these two approaches tend to be small for diamond-type crystals, but larger for III-V and II-VI compounds, particularly when the constituent atoms belong to different rows of the Periodic Table.[3] In short, this distinction should *not* lead to significant differences *vis a vis* the present work and that of Rudge.[17]

(b) In OPW band calculations,[17,32-35] the core orbitals are determined in a spherically averaged cellular potential, but the valence- and conduction-band wave functions are determined for a crystal potential which includes nonspherical as well as spherical components. In the present work, the crystal potential is spherically averaged in the atomic (and interstitial) polyhedra. As shown by Williams and Morgan,[30] the neglect of nonspherical components of the crystal potential can introduce errors as large as a few eV in the band structure of silicon. In our calculations for diamond, these errors should be considerably smaller for fourfold than for twofold partitioning since the cells are more nearly spherical in shape.

V. KIMBALL SOLUTION BASED ON TWOFOLD PARTITIONING

Kimball's pioneering cellular calculation for the diamond crystal[3] was based on a twofold partitioning of the unit cell, which leads to atomic polyhedra of the type shown in Fig. 2. Kimball expanded the crystal wave function in terms of s, p_x, p_y, and p_z functions in each of the two polyhedra, so that the basis set consisted of $2 \times 4 = 8$ atomiclike functions. He used the centers of the hexagonal faces as matching points. There are eight such points, and we will call these the Kimball points.

Using our own crystal potential, we recalculated the band structure of diamond using Kimball's model (preceding paragraph). The energy bands along the [100] and [111] directions in the reduced zone are shown in Fig. 4. For these high-symmetry directions, the 8×8 determinantal equation can be factored analytically, and the energy eigenvalues can be expressed in terms of the values of the radial wave functions (s and p) and their derivatives (s' and p') at the matching points. For example, at the zone center, the solutions for Γ_1, $\Gamma_{25'}$, Γ_{15}, and $\Gamma_{2'}$ are determined, respectively, by the following conditions: $s'/s = 0$, $p'/p = 0$, $p/p' = 0$, and $s/s' = 0$. The twofold degenerate bands along the [100] and [111] axes are flat because the relevant subdeterminants are independent of $\vec{k}$ along these directions.

Apart from the flatness of the topmost valence bands and bottommost conduction bands, the energy-band structure shown in Fig. 4 is qualitatively reasonable, and bears a striking resemblance to that given by Hall's nearest-neighbor LCAO scheme.[36] The lowest conduction-band level at

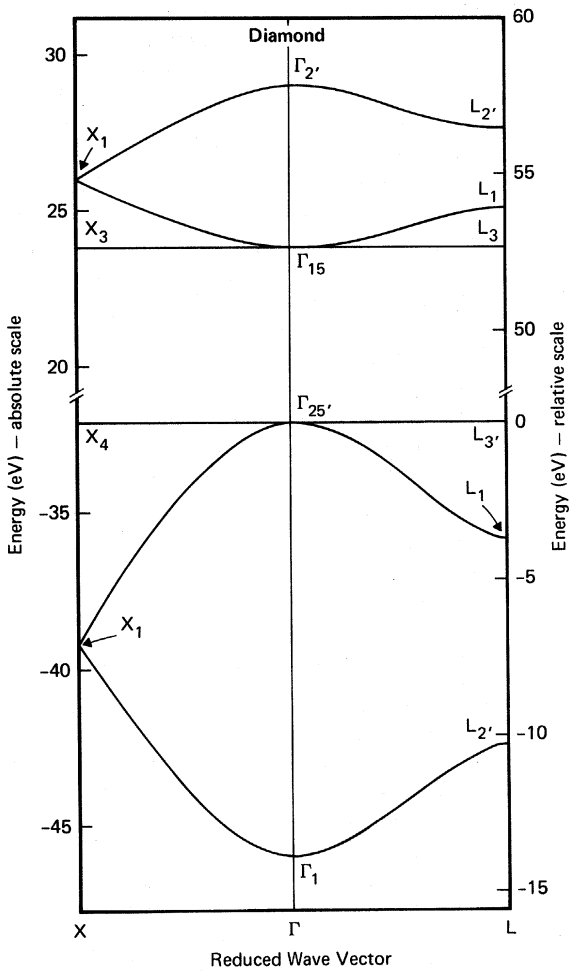

FIG. 4. Energy-band structure of diamond based on twofold partitioning and matching at the Kimball points. Apart from the different choice of cellular potentials, this solution corresponds to Kimball's original solution (cf. Fig. 3). The total number of basis functions used is eight.

the zone center is Γ_{15}, in agreement with OPW results.[11,12,17] The principal shortcoming of the cellular solution is the extremely large (53 eV) energy separation between the highest valence bands and the lowest conduction bands. This deficiency can be attributed to the limited number of basis functions used, or, what amounts to the same thing, the limited number of matching points used.

In a related context, von der Lage and Bethe[10] argued that the choice of the centers of hexagonal faces as matching points is particularly bad, first, because these points are much closer to the nucleus than an average point on the cell boundary, and second, because the higher symmetry makes the boundary conditions degenerate. Von der Lage and Bethe recommended the use of the intersections of adjacent equivalent-volume spheres, rather than the tangency points of inscribed spheres, as the matching regions.

In the present application to the diamond crystal, the principal reason for the large gap is the inadequacy of the basis set. Of course, by using a small basis set, we are obliged to use the Kimball points, which suffer from the difficulty already pointed out by von der Lage and Bethe.

The consequences of introducing more basis functions and more matching points will be investigated in the next three sections.

VI. GENERALIZED KIMBALL SOLUTION BASED ON FOURFOLD PARTITIONING OF UNIT CELL

We will now consider a generalized version of Kimball's original solution based on the decomposition of the unit cell into two atomic and two interstitial (or vacancy) polyhedra (cf. Fig. 3). As matching points we will choose the centers of the hexagonal faces of the four polyhedra, and we will again call these the Kimball points. There are clearly $8\times4=32$ Kimball points. Accordingly, we require 32 basis functions, that is, eight basis functions per polyhedron.

If we use all spherical harmonics up to and including some maximum value l_{max}, we cannot get eight basis functions per polyhedron. Instead, we will use a carefully selected set of s, p, d, and f functions, which together provide a "balanced" representation for the valence and lower conduction bands along the [100] and [111] axes. In particular, we will use the following set of tetrahedral (symmetry-adapted) harmonics: s-type: 1; p-type: $x/r, y/r, z/r$; d-type: $xy/r^2, yz/r^2, zx/r^2$; f-type: xyz/r^3. (Such harmonics are thoroughly discussed by von der Lage and Bethe.[10]) The band structure determined along the [100] and [111] axes for this choice of basis functions and matching points is shown in Fig. 5.

By increasing the total number of basis functions and matching points from eight to 32, the width of the forbidden band is reduced substantially, from over 50 to about 15 eV. The experimental value is 5.4 eV.[26,27] The width of the valence bands is reduced slightly, from about 14 to 12 eV. The experimental value is 24.2 eV.[28] The highest valence band remains rather flat, while the four lowest conduction bands come closer together, with Γ_2' falling slightly below Γ_{15}.

From the standpoint of a first-principles solution, the band structure shown in Fig. 5 is still a disappointment. It is reasonable to conclude that 32 basis functions per unit cell are still not sufficient to provide a quantitatively acceptable solution for the band structure of diamond.

Nevertheless, the analytical form of the 32×32 determinantal equation is still sufficiently simple to make possible the expression of various key solutions in algebraic form. In Table I we compare the analytical expressions for certain energy levels as given by the original Kimball model (Sec. V) and by the extended Kimball model (present section). Clearly, the various logarithmic derivatives, s'/s, p'/p, d'/d, and f'/f, can be expressed as algebraic functions of energy and suitably parametrized, providing simple and instructive models of the band structure of diamond (and related crystals). The feasibility of this type

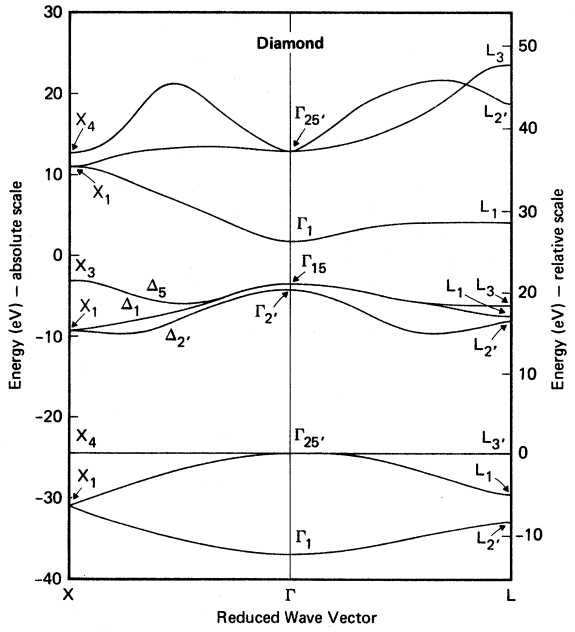

FIG. 5. Energy-band structure of diamond based on fourfold partitioning and matching at the Kimball points. The total number of basis functions used is 32.

of parameterization has recently been explored and successfully demonstrated in the context of Korringa-Kohn-Rostoker (KKR) band-structure calculations.[37,38]

One interesting feature of Table I is that ratios such as s'/s appear one way for twofold partitioning and in reciprocal form for fourfold partitioning (for a given energy level). It is instructive to draw simple wave-function pictures for the various symmetry types and confirm these algebraic relations (we leave this to the reader as an exercise). Another interesting feature of Table I is the degeneracy of $\Gamma_{25'}$, X_4, and of Γ_{15}, X_3 for both types of partitioning. With twofold partitioning, the bands connecting these pairs are flat (cf. Fig. 4), while for fourfold partitioning, the bands are not necessarily flat (cf. Fig. 5). Nevertheless, the degeneracy of the Γ and X solutions represents an inherent limitation in the flexibility of these models, a limitation associated with the use of the Kimball points for matching. In order to obtain more realistic band structures, e.g., nonflat doubly degenerate bands along the [100] axis, it is necessary to use other (or additional) matching points. For example, with fourfold partitioning, one could include the six square face centers for each polyhedron, as well as the following six tetrahedral harmonics: d-type: $(x^2-y^2)/r^2$, $[z^2-\frac{1}{2}(x^2-y^2)]/r^2$; f-type: x^3/r^3, y^3/r^3, z^3/r^3; g-type: $(x^4+y^4+z^4)/r^4$. This would increase the number of logarithmic derivatives by one (g'/g), and increase the order of the determinantal equations from 32 to 56, still a manageable number.

TABLE I. Analytical expressions for selected energy levels corresponding to the solutions shown in Figs. 4 and 5. The radial wave functions and their normal derivatives are evaluated at the Kimball points of atomic polyhedra (subscript a) and interstitial polyhedra (subscript i).

Energy level	Twofold partitioning (cf. Fig. 4)	Fourfold partitioning (cf. Fig. 5)
Γ_1	$\frac{s_a'}{s_a}=0$	$\frac{s_a}{s_a'}+\frac{f_a}{f_a'}+\frac{s_i}{s_i'}+\frac{f_i}{f_i'}=0$
$\Gamma_{2'}$	$\frac{s_a}{s_a'}=0$	$\frac{s_a'}{s_a}+\frac{f_a'}{f_a}+\frac{s_i'}{s_i}+\frac{f_i'}{f_i}=0$
$\Gamma_{25'}$ X_4	$\frac{p_a'}{p_a}=0$	$\frac{p_a}{p_a'}+\frac{d_a}{d_a'}+\frac{p_i}{p_i'}+\frac{d_i}{d_i'}=0$
Γ_{15} X_3	$\frac{p_a}{p_a'}=0$	$\frac{p_a'}{p_a}+\frac{d_a'}{d_a}+\frac{p_i'}{p_i}+\frac{d_i'}{d_i}=0$

VII. IMPROVED CELLULAR SOLUTIONS BASED ON TWOFOLD PARTITIONING

We will now return to twofold partitioning and attempt to improve on Kimball's original solution by introducing more basis functions and more matching points. It is through the choice of these quantities that one conveys all the information about the symmetry of the crystal and the spatial characteristics of the cellular basis functions. The actual choice of matching points is clearly arbitrary. However, care should be taken to ensure that a particular choice of matching points is compatible with the choice of basis functions. It is particularly important to avoid introducing redundant boundary conditions, which would lead to null determinants. Such redundancies can arise, for example, if matching points are placed at symmetry positions on the cell faces, and two or more boundary conditions become degenerate for these particular positions and the particular choice of basis functions. It is also most important to avoid nearly redundant boundary conditions, which lead to poorly conditioned determinants and hence to numerical instability. This can be avoided by not placing the matching points too closely together.

Since most of the surface of the atomic polyhedron is accounted for by the four hexagonal faces (cf. Fig. 2), we will confine our attention to these faces in what follows, ignoring the small triangular faces which connect next-nearest neighbors. Beginning with an arbitrary point on one of the hexagonal faces, and applying all the symmetry operations of the factor group of the diamond space group (O_h^7), we generate a set of 48 symmetrically equivalent points. There are six points on each of the eight hexagonal faces of the two atomic polyhedra.

Associated with these 48 symmetry-related points are 48 additional points connected to the former by $\vec{R}=(0,0,0)$ and the three primitive translation vectors of the direct lattice. These 48 additional points are generated by the boundary conditions [cf. Eqs. (2) and (3)].

The general pattern of points on one particular hexagonal face of the atomic polyhedron is shown in Fig. 6. The circles represent symmetry-generated points, and the squares, boundary-condition-generated points. For each of the "circle" points, there is a "square" point; these are called conjugate points and are related to one another by inversion through the Kimball point. The total number of general points is clearly $48+48=96$. If the original point lies on one of the symmetry lines of the hexagonal face, pairs of points coalesce and the total number of points

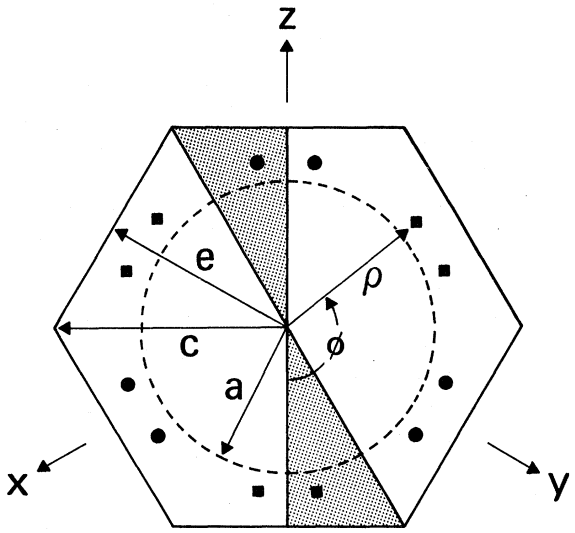

FIG. 6. Notation for hexagonal faces of capped tetrahedra (cf. Fig. 2) and truncated octahedra (cf. Fig. 3). The face center is the Kimball point in both cases. Matching points are denoted by radius ρ and azimuthal angle ϕ. Symmetry-generated points are denoted by circles, and boundary-condition-generated points by squares. The irreducible sector is shown shaded. The radius of the von der Lage and Bethe circle (shown for twofold partitioning) is denoted by a. The distances to the corner and to the midpoint of an edge are denoted by c and e. If drawn on the same scale, the radius of the von der Lage and Bethe circle for fourfold partitioning would be about 6% larger than that for twofold partitioning. For twofold and fourfold partitioning, respectively, $a=0.222$ and 0.117, $c=0.353$ and 0.177, and $e=0.306$ and 0.153, all in units of a_L. The lattice constant used for diamond was $a_L=3.5597$Å.

is 48. If the Kimball point serves as the original point, the total number is eight.

If more than one set of points is used, the total number of matching points will be equal to $N=8A+48B+96C$, where A is 1 or 0 depending on whether the Kimball points are used, B is the number of different types of points lying on symmetry lines, and C is the number of different types of points lying at general positions on the hexagonal faces. In order to satisfy all the boundary conditions, a corresponding number of basis functions must be introduced. As in Sec. VI, it will usually not be possible to include all spherical harmonics (or tetrahedral harmonics) up to and including some $l_{\max}$ and have this number of harmonics come out exactly equal to the total number of matching points. Accordingly, one must tailor-make the basis set to suit the circumstances, allowing for the fact that symmetrization (see below) should lead to compatible numbers of symmetrized basis functions and matching points for all symmetry species.

Having chosen one or more sets of matching points, we can specialize to some point in the reduced zone and factor the determinantal equation into symmetrized determinantal equations, one corresponding to each irreducible representation of the group of the wave vector $\vec{k}$. In doing this, we find it convenient to use tetrahedral harmonics as the basis functions, rather than the standard spherical harmonics. Tetrahedral harmonics are linear combinations of spherical harmonics which transform according to the irreducible representations of the tetrahedral point group T_d, which describes the atomic site symmetry. A convenient compilation of tetrahedral harmonics has been published by Altmann and Cracknell,[39] whose tables we have used extensively in the present work.

When the original determinantal equation for a point of high symmetry in the reduced zone is factored into symmetrized subdeterminantal equations, a general set of matching points (e.g., 96 points) is often reduced to a small number of inequivalent matching points.[40] For example, at Γ and X, a set of 96 points is reduced to one pair of "conjugate" matching points lying in one irreducible sector of the hexagonal face common to both atomic polyhedra, i.e., one circle point and one square point in the shaded region of Fig. 6. For L, a set of 96 points reduces to the above conjugate pair plus another pair of conjugate points lying on one of the exterior faces of either atomic polyhedron.

In order to take maximum advantage of symmetry, we have confined our studies to the Γ, X, and L points in the reduced zone. It is known from previous OPW band-structure calculations for diamond-type crystals[33-35] that the band structure throughout the reduced zone can be determined simply from a knowledge of the energy levels at Γ, X, and L by making use of a pseudopotential interpolation scheme. Thus, the information we obtain at Γ, X, and L is actually sufficient to map out the band structure throughout the entire reduced zone if we wished to do so. However, within the present context, our principal objective is to determine the convergence properties of the energy levels (at Γ, X, and L) as a function of the number and location of the matching points employed.

The results of such convergence studies for the center of the reduced zone are shown in Figs. 7–10. In these drawings, the calculated energy levels are shown as a function of the choice of matching points, for various tetrahedral harmonic expansions. The abscissa is ρ/a, where ρ is the distance from the Kimball point to the most distant

TABLE II. Matching points used in selected calculations for $\Gamma_{25'}$ and Γ_{15} based on twofold partitioning. The matching points are identified by their radii and azimuthal angles (cf. Fig. 6). Only one member of each conjugate pair of matching points is listed. An asterisk next to l_{max} signifies that all matching points for lower values of l_{max} are already included, and that only the additional matching points are actually listed. For $l_{max}=12$ all matching points (one per conjugate pair) are listed. Energy levels are expressed in Ry.

		Matching points		Energy levels		
l_{max}	Dimensionality of symmetrized matrix	Radius ρ (in units of a)	Azimuthal angle ϕ (deg)	Γ_{15}	$\Gamma_{25'}$	$\Gamma_{15}-\Gamma_{25'}$
2	2	1.0	0	−1.88	−0.95	−0.93
3*	3	0.0	0	−1.08	−1.47	−0.39
5*	5	1.0	7.5	−0.90	−1.18	0.28
7*	9	1.0	15	−0.68	−1.18	0.50
		0.75	0			
8*	11	0.75	7.5	−0.68	−1.18	0.50
12	24	1.35	0			
		1.35	7.5			
		1.35	15			
		1.35	22.5			
		1.25	0	−0.68	−1.18	0.50
		1.25	7.5			
		1.25	15			
		1.25	22.5			
		1.0	0			
		1.0	7.5			
		1.0	15			
		0.25	0			

matching point used in the same face, and a is the radius of the von der Lage and Bethe circle (cf. Sec. I and Fig. 6).

When a given solution involves several inequivalent matching points, their azimuthal positions are held fixed and the various values of ρ are varied. Although the pattern of matching points is maintained, the radii of the inner matching points are not necessarily scaled in proportion to the radius of the outermost matching point (or points). Representative selections of matching points for $\Gamma_{25'}$ and Γ_{15} are listed in Table II.

The calculations for Γ_1 and $\Gamma_{2'}$ were carried out up to $l_{max}=8$. As can be seen from Fig. 7, the calculated energy eigenvalues are strongly dependent on the position of the maximum matching radius for the lower values of l_{max}. The behavior of Γ_1 is particularly interesting. For $l_{max}=4$ and 6, the two lowest solutions for Γ_1 coalesce for small values of ρ/a, and separate for large values. Thus, it is possible to obtain spurious solutions if such anomalous behavior is not recognized. It is easy to appreciate the difficulties that some of the earlier investigators encountered when they attempted to carry out cellular calculations using too few spherical harmonics.

On the other hand, when a sufficiently large number of spherical (or tetrahedral) harmonics are introduced, the calculated eigenvalues become rather insensitive to the choice of matching points. For Γ_1 and $\Gamma_{2'}$, it is necessary to go up to $l_{max}=8$ and 6, respectively, to obtain nearly convergent energy levels (where convergent means independent of matching points).

Our results for $\Gamma_{25'}$ and Γ_{15} are shown in Figs. 8 and 9. In Fig. 8 we concentrate on $\Gamma_{25'}$ and show the location of a converged value of Γ_{15} for reference, while in Fig. 9 we do the opposite. For lower values of l_{max}, there is again substantial variation of the eigenvalues with the choice of matching points. For $l_{max}=3$ or 5, it is possible to obtain a widely different range of values for the direct band gap ($\Gamma_{15}-\Gamma_{25'}$) simply by choosing different matching points. But, once again, for sufficiently large values of l_{max} (here $l_{max}\geq 7$), the energy levels become relatively insensitive to the choice of matching points.

We believe that even if the boundary conditions were to be satisfied in a least-squares sense over all the polyhedral faces, one could still obtain spurious results if an insufficient number of basis functions were used.

Our results for $\Gamma_{12'}$ are displayed in Fig. 10.

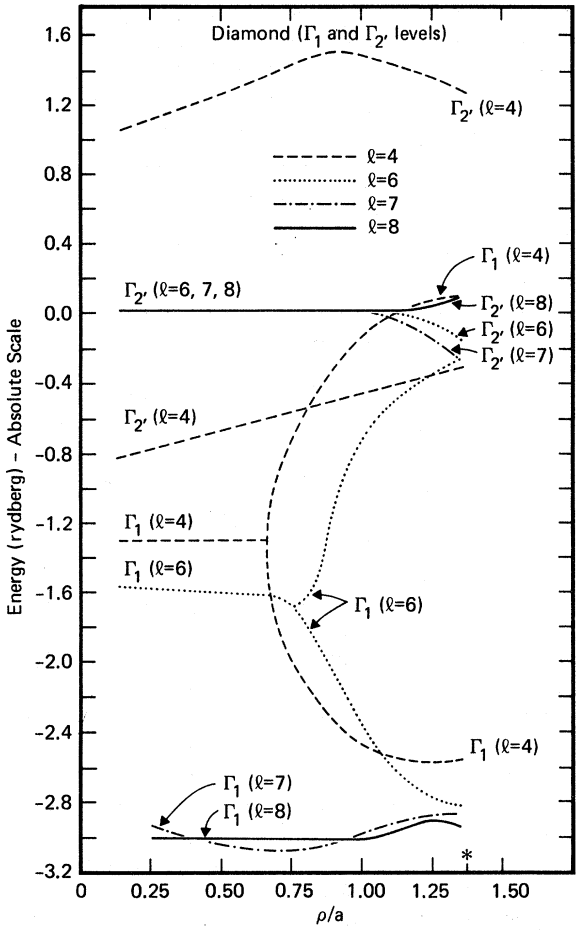

FIG. 7. Convergence study for Γ_1 and $\Gamma_{2'}$ based on twofold partitioning and various choice of l_{max} (denoted here by l). The calculated energy levels are plotted as a function of the radius of the matching point most distant from the Kimball point, i.e., the matching point with the largest value of ρ. Where two Γ_1 solutions occur, they correspond to valence- and conduction-band levels. The abscissa corresponding to $\rho = e$ is denoted by an asterisk.

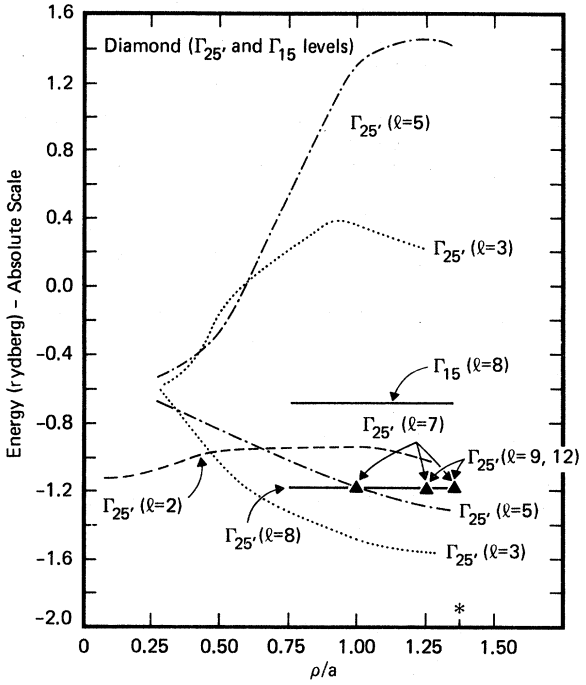

FIG. 8. Convergence study for $\Gamma_{25'}$ based on twofold partitioning. A converged value for Γ_{15} is shown for reference. Where two $\Gamma_{25'}$ solutions occur, they correspond to valence- and conduction-band levels. The abscissa corresponding to $\rho = e$ is denoted by an asterisk.

For $l_{max} = 4$, 6, and 10, the energy levels are determined for a wide range of matching points. For $l_{max} = 8$ and 11, only a limited number of calculations were carried out. It is difficult to say whether we have obtained convergent energy levels even with $l_{max} = 11$. However, since $\Gamma_{12'}$ represents a rather high-lying conduction-band level, our result for $l_{max} = 11$ provides an acceptable estimate.

We have also investigated the convergence properties of the energy levels at X and L. Since the wave-function symmetry is lower at X and L than at the zone center, it is necessary to use larger basis sets and more matching points. If we were to go to extremely large numbers of matching points, they would get so close together

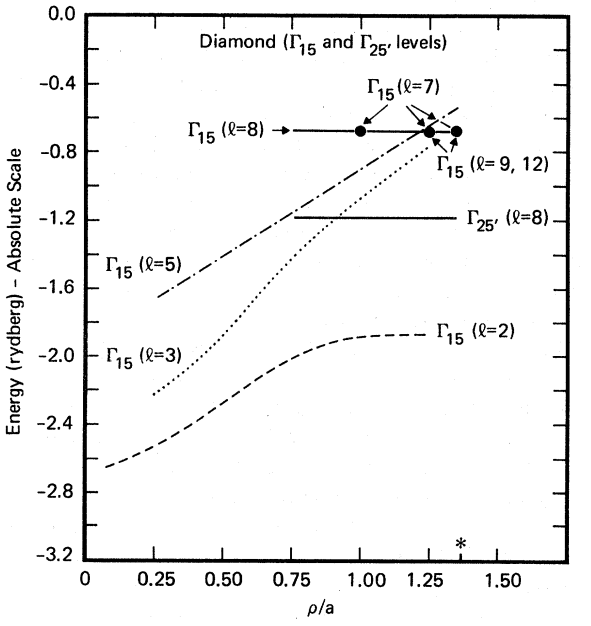

FIG. 9. Convergence study for Γ_{15} based on twofold partitioning. A converged value for $\Gamma_{25'}$ is shown for reference. The abscissa corresponding to $\rho = e$ is denoted by an asterisk.

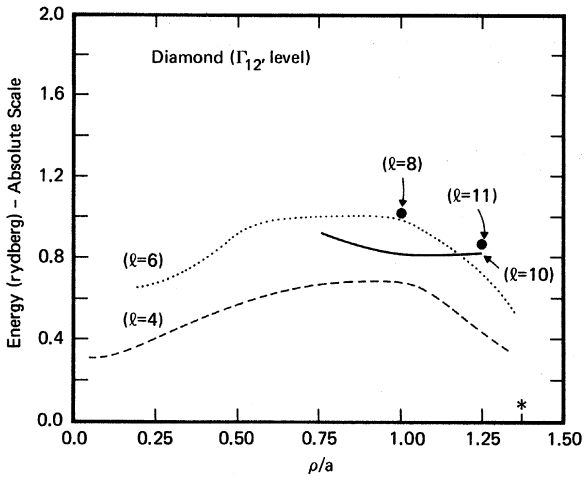

FIG. 10. Convergence study for $\Gamma_{12'}$ based on twofold partitioning. The abscissa corresponding to $\rho = e$ is denoted by an asterisk.

that calculations based on isolated-point matching would become impractical. Fortunately, we did not reach this limit when we carried out calculations at X and L for $l_{max} = 8$, 9, 10, and 12. Although our convergence studies at X and L were not as comprehensive as they were for Γ, we believe that we have obtained reasonably good estimates of the principal energy levels at these zone points (say, estimates good to a fraction of an eV).

In Table III our present results for Γ, X, and L are compared with some recent OPW results due to Rudge[17] and Euwema and Stukel,[41] and with relevant experimental information. Rudge's OPW calculations used 331 OPW's at Γ and 302 at X and L. Euwema and Stukel studied the convergence properties of the Γ solutions using as many as 965 OPW's (for which we quote their results). Since the same physical model (crystal potential) is employed by Rudge and by Euwema and Stukel, it is gratifying that their results agree with one another for 331 OPW's.

It is clear from Ref. 41, that individual OPW energy levels for diamond are not fully convergent at 331 OPW's, or even at 965 OPW's. Nevertheless, it is possible to make reliable estimates of the band structure by taking the differences between pairs of energy levels, since these differences converge more rapidly than the individual levels do. In Table III, we have set the top of the valence band ($\Gamma_{25'}$) to 0 for the purpose of comparing different theoretical energy-level calculations. Thus, we are comparing energy-level differences rather than absolute energies. Based on a comparison of the OPW results of Refs. 17 and 41, we believe that Rudge's energy differences at Γ, X, and L are convergent to within an eV.

It is interesting to note that our best cellular calculations for $\Gamma_{25'}$ and Γ_{15} involve approximately as many basis functions as are used in Rudge's OPW band calculations. According to Table II, for $l_{max} = 8$, we use two general sets of matching points (2×96), two special sets (2×48), and one set of Kimball points (1×8), making a total of 296 matching points. This leads to 296 basis functions (tetrahedral harmonics), which is comparable to the number of OPW's (331) used by Rudge.

Of course, the 296×296 cellular determinant can be factored into subdeterminants by standard group-theoretical methods, and these can be evaluated separately. We took full advantage of symmetry factoring in the present studies. For example, for $\Gamma_{25'}$ and Γ_{15} with $l_{max} = 8$, we had to deal with 11×11 subdeterminants.

As can be seen from Table III, the improved cellular results (twofold partitioning) are considerably closer to experiment (and to the OPW results) than were the earlier Kimball-point solutions (cf. Secs. V and VI). Both the cellular and the OPW calculations indicate that the Γ_{15} conduction-band level lies considerably below the $\Gamma_{2'}$ conduction-band level, contrary to recent nonlocal-empirical-pseudopotential calculations.[20]

The improved cellular results at X and L (twofold partitioning) are considerably more realistic than were the solutions given earlier in Secs. V and VI. However, there are still significant discrepancies between the cellular and OPW results. In particular the lower conduction-band and upper valence-band levels at X and L lie considerably lower than they should, relative to their counterparts at Γ. As will be seen, most of these discrepancies can be reduced considerably by going to fourfold partitioning.

VIII. IMPROVED CELLULAR SOLUTIONS BASED ON FOURFOLD PARTITIONING

No matter how many basis functions we use with twofold partitioning, we cannot get around the fact that the spherical approximation for the crystal potential is not likely to be as good for twofold as it is for fourfold partitioning. Instead of attempting to introduce the nonspherical part of the crystal potential into the atomic polyhedra of Fig. 2, we will retain the spherical-cellular-potential approximation and carry out a convergence study based on the fourfold partitioning scheme.

We are now dealing with truncated octahedra (cf. Fig. 3) which have eight hexagonal faces and

TABLE III. Comparison of theoretical and experimental energies for diamond. The present cellular calculations and both OPW band calculations are based on Slater's exchange approximation ($\alpha = 1$). The letters c and v distinguish conduction- and valence-band levels. In all the calculations, the zero of energy has been placed at the top of the valence bands ($\Gamma_{25'c}$). All entries are in eV.

Energy levels and principal gaps	Cellular calculations		OPW calculations		
	Twofold partitioning	Fourfold partitioning	Rudge (Ref. 17)	Euwema and Stukel (Ref. 41)	Experiment
$\Gamma_{12'}$ (c)	28.3		26.8		
Γ_1 (c)			19.7		
$\Gamma_{2'}$ (c)	16.3	19.7	12.0	12.5	
Γ_{15} (c)	6.8	6.3	6.5	6.3	7 – 7.3 [a]
$\Gamma_{25'}$ (c)	0.0	0.0	0.0	0.0	
Γ_1 (v)	−24.8	−21.9	−22.3		−24.2 [b]
X_3 (c)	7.9		18.8		
X_1 (c)	1.1	4.9	5.1		~6 [c]
X_4 (v)	−14.5	−8.7	−6.1		
X_1 (v)	−18.6	−14.1	−13.5		
$X_{3c} - X_{4v}$	22.4		24.9		
$X_{1c} - X_{4v}$	15.6	13.6	11.2		~12 [d]
$L_{2'}$ (c)	18.8		17.4		
L_3 (c)			9.4		
L_1 (c)	5.2		8.1		
$L_{3'}$ (c)	−11.1		−2.6		
L_1 (v)	−19.9		−13.4		
$L_{2'}$ (v)	−22.7		−16.8		
$L_{3c} - L_{3'v}$			12.0 [e]		
$L_{1c} - L_{3'v}$	16.3		10.7 [e]		

[a] Direct band gap, Refs. 26 and 27.

[b] Width of valence bands, Ref. 28.

[c] According to Refs. 26 and 27, the indirect band gap is 5.46 eV. Our best estimate places X_1 about 0.5 eV above the lowest conduction-band level Δ_1. Therefore, X_1 is about 6 eV above $\Gamma_{25'}$, as indicated.

[d] Reference 25. The experimental optical spectrum has been analyzed by several investigators; see, for example, Refs. 18–20.

[e] These results are consistent with the view, expressed earlier in Ref. 12, that the two L peaks contribute to the main optical peak at 12 eV. The major contribution to the main peak is due to the X-Σ region.

six square faces. Since adjacent carbon atoms interface one another across hexagonal faces, we would expect these faces to be more important than the square faces in the limit of relatively few matching points. Accordingly, we will restrict our attention to the hexagonal faces, one of which is shown in Fig. 6. The equivalent-volume sphere is now $\frac{1}{2}$ as large as before, and its radius is $(\frac{1}{2})^{1/3}$ as large as before.

If we choose the generic matching point at a general position on a hexagonal face belonging to a particular polyhedron, the 48 operations of the factor group of the space group O_h^7 will generate a set of 48 symmetrically equivalent points which lie on the hexagonal faces of this and a neighboring polyhedron. This procedure is carried out once for each of the four polyhedra, leading to $4 \times 48 = 192$ distinct points. Accompanying these are an equal number of points generated by the boundary conditions, making a grand total of $2 \times 192 = 384$ points. The general pattern of points on a hexagonal face of the truncated octahedron is shown in Fig. 6, which we have already encountered in Sec. VII and which is readily adapted to the present context. The total number of points is reduced from 384 to 192 if the generic point lies on a symmetry line, and to 32 if the generic point lies at the face center (Kimball point).

We will confine our attention to Γ and X since convergence studies for these two zone points are sufficient to provide meaningful comparisons with the results of Sec. VII. As before, we will use

tetrahedral harmonics as basis functions and factor the determinantal matrices for each zone point into smaller symmetrized matrices which can be evaluated separately. The symmetrized matrices for Γ and X involve only the irreducible sectors of five hexagonal faces of four polyhedra. Three of these faces are the interfaces between adjacent carbon-carbon, carbon-interstitial, and interstitial-interstitial polyhedra (cf. Fig. 3). The remaining two faces connect the carbon polyhedron centered at (0, 0, 0) with the interstitial polyhedron centered at $a_L(\frac{3}{4}, \frac{3}{4}, \frac{3}{4})$. We used five such faces all of which were perpendicular to the unit cube diagonal, i.e., to the (1, 1, 1) axis.

In the present series of convergence studies, the energy levels were calculated for each symmetry species for progressively larger values of l_{max}. The variation of the calculated energy levels was investigated as a function of the choice of matching radius for various values of l_{max} only for $\Gamma_{25'}$ and Γ_{15}. The results of the studies for $\Gamma_{25'}$ and Γ_{15} are shown in Figs. 11 and 12. The calculated energy levels are seen to be relatively insensitive to the matching radius once l_{max} is equal to or greater than 8. For $l_{max} = 8$, the energy levels vary by less than 0.05 Ry for various choices of matching radius.

It is interesting to note that the $\Gamma_{25'}$ and Γ_{15} solutions converged at about $l_{max} = 8$ for both twofold and fourfold partitioning. Thus, the convergence properties are not significantly affected by the differences in the number and form of the cellular polyhedra. Since there are twice as many basis functions for fourfold than for twofold partitioning, for a common value of l_{max}, it takes more effort to obtain comparable convergence using fourfold partitioning. In return for this extra effort one has a more accurate approximation for the crystal potential in the interstitial regions. As mentioned earlier, the principal advantage of fourfold partitioning is the reduction in the errors associated with the neglect of nonspherical-cellular-potential components.

We did not investigate the variation of the energy levels for Γ_1, $\Gamma_{2'}$, X_1, or X_4 with matching radius. Instead, we carried out calculations using $l_{max} = 10$ and representative matching radii. All of our numerical results for Γ and X are listed in Table III. Based on our experience with twofold partitioning, we believe that the present results for Γ are convergent to within 1 eV, and those for X to within a few eV. The following features of Table III should be noted:

(a) Both twofold and fourfold partitioning lead to forbidden bandwidths at the zone center ($\Gamma_{15} - \Gamma_{25'}$) and to valence bandwidths ($\Gamma_{25'} - \Gamma_1$) which compare favorably with experiment and are in reasonable agreement with the OPW results.

(b) We are not able to account for the behavior of $\Gamma_{2'}$, which is in better agreement with the OPW results for twofold than for fourfold partitioning.

(c) Fourfold partitioning leads to a distinct improvement in the energy-level structure at X. (The same would be expected for L.) The lowest conduction-band level (X_1) and the valence-band levels (X_4 and X_1) all move closer to their experimental (and OPW) counterparts. The improved cellular results based on fourfold partitioning yield numerical results for the indirect band gap (about 4.5 eV) and for the energy of the main optical peak (about 13.6 eV) which are within 1 or 2 eV of their experimental values. Such results are gratifying for a first-principles band-structure calculation.

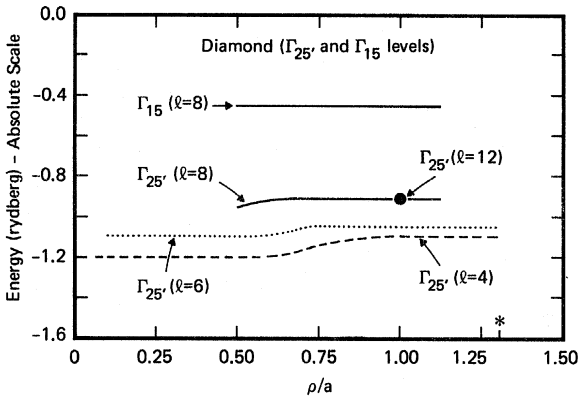

FIG. 11. Convergence study for $\Gamma_{25'}$ based on fourfold partitioning. A converged value for Γ_{15} is shown for reference. The abscissa corresponding to $\rho = e$ is denoted by an asterisk.

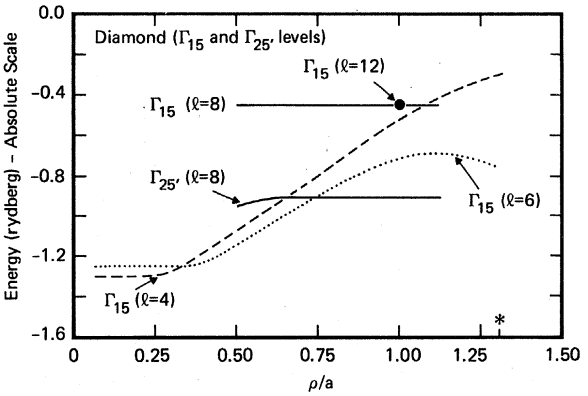

FIG. 12. Convergence study for Γ_{15} based on fourfold partitioning. A converged value for $\Gamma_{25'}$ is shown for reference. The abscissa corresponding to $\rho = e$ is denoted by an asterisk.

(d) In going from twofold to fourfold partitioning, there is a considerably greater change in the band structure in the exterior region of the reduced zone (as exemplified by the zone point X) than at the center of the zone. We believe that this effect is produced by the respective spherical-cellular-potential approximations. The improved representation of the crystal potential brought about by fourfold partitioning leads to improved relative positions of the energy levels at Γ and X.

Considering the distinct lack of success of previous efforts to apply the cellular method to diamond-type crystals using isolated matching points[3-8] as well as more sophisticated techniques,[9] it is indeed gratifying that the present results (particularly with fourfold partitioning) agree with experiment and with OPW band calculations as well as they do. The two essential improvements inherent in our work are the use of a sufficient number of basis functions and matching points to ensure a reasonable degree of energy-level convergence, and, through fourfold partitioning, an improved approximation to the crystal potential in about $\frac{2}{3}$ of the unit cell.

The present results could be improved still further by taking the nonspherical part of the cellular potential into account, by carrying out the calculations self-consistently, and possibly also by including matching points on the square faces of the truncated octahedra. However, these refinements lie outside the scope of the present study.

IX. DISCUSSION

We have demonstrated that the cellular method based on point matching leads to energy levels that are relatively insensitive to the choice and spatial arrangement of a limited number of matching points, provided the cellular wave functions are represented by a sufficiently large number of basis functions. Many of the earlier workers[3-9] encountered difficulties with the cellular method because they used too few basis functions.

Moreover, we have demonstrated that so long as a sufficiently large number of basis functions is employed, it is possible to obtain substantially the same energy-level structure by satisfying the boundary conditions over different limited regions of the polyhedral surfaces. However, it is important that the matching regions be suitably chosen.

For example, with twofold partitioning, it is necessary for the matching points to be located on two or more circles on each of the hexagonal faces of the atomic polyhedron. (One of these circles can have zero radius and thus degenerate to the Kimball point.) If the points lie on only one circle per hexagonal face, the basis functions will not mix properly, and spurious solutions will be obtained.

With twofold partitioning, reasonable results can be obtained by satisfying the boundary conditions at points lying on a minimum of two well-separated circles on each of the hexagonal faces. For the calculated energy-level structure to become nearly independent of the number and location of the matching points (subject to this restriction), it is necessary to include all tetrahedral harmonics up to $l_{max}=7$ or 8 at the zone center, and up to $l_{max}=11$ or 12 at X and L.

With fourfold partitioning, correspondingly good results can be obtained by satisfying the boundary conditions on only one circle per hexagonal face. (There are $8\times4=32$ such faces for this case.) Even though the unit cell has been divided into twice as many subcells as before, the minimum number of spherical harmonics required for convergence is about the same (in total) as before.

Although we have demonstrated the insensitivity of the calculated energy levels to the choice of matching points, provided a sufficiently large basis set is used, we have not demonstrated (or in fact examined) the relationship between the calculated eigenvector components and the choice of matching points. We are not presently in a position to say to what extent the eigenfunctions and their normal derivatives satisfy the boundary conditions at points well removed from the matching points.

Of course, the insensitivity of the energy levels to the choice of matching points does not guarantee comparable insensitivity of the spherical-harmonic expansion coefficients to this choice. However, it is difficult to imagine eigenfunctions whose expansion coefficients are strongly dependent on the choice of matching points, and yet whose energy eigenvalues are only weakly dependent on this choice. It is reasonable to expect the imposition of strict boundary conditions on one circle (i.e., at points located on one circle) to limit greatly the form of the wave function on neighboring circles. Thus, if the matching circles are suitably chosen, it is conceivable that the restraints imposed on the wave functions will tend to minimize the variation of their expansion coefficients with respect to the choice of matching circle.

In order to minimize the variation of the wave functions with respect to the choice of matching points, it is probably desirable to choose a matching circle that samples the most representative region of the hexagonal face. This would exclude extremely small circles, which sample only a

very small fraction of the hexagonal face. Von der Lage and Bethe have already suggested the use of the circles defined by the intersection of neighboring equivalent-volume spheres as appropriate average matching circles.[10]

The choice of optimum matching circles in the present context is reminiscent of the use of Baldereschi points[42-45] in summations over the reduced zone. If, for example, in self-consistent band-structure calculations for diamond-type crystals, one samples the valence charge density only at the zone center, the self-consistent valence charge density obtained is considerably different from that given by more extensive sampling of the reduced zone. If one uses the L point instead of the Γ point, the final charge density is considerably closer to that obtained by more complete sampling. This follows from the fact that the L point is more representative of the reduced zone as a whole than is the Γ point.

Now Baldereschi[42] and others[43,44] have shown that the sum over a large number of uniformly distributed points in the reduced zone can be approximated quite well by using a very small number of carefully chosen representative points (Baldereschi points). Phillips[45] has argued that these points may have physical significance over and above their mathematical significance as "mean-value" points.

By analogy, it is possible that an optimum match over the entire surface of a Wigner-Seitz polyhedron can be accomplished by a suitable choice of matching-sphere radius (or radii). This possibility deserves further study.

ACKNOWLEDGMENTS

One of the authors (J.R.L.) wishes to thank the IBM World Trade Corp. and IBM Brazil for their encouragement and financial support. The work reported here was carried out by J.R.L. under a World Trade Fellowship. The authors are grateful to Dr. William E. Rudge for his interest and advice, and for providing results of unpublished OPW band calculations for diamond. We are also grateful to Dr. Rudge and Dr. Inder P. Batra for their critical reading of the manuscript.

---

*Present address: Departmento de Física dos Materiais e Mecanica, Instituto de Fisica, Universidade de Sao Paulo, Cidade Universitaria, Caixa Postal 20516, Sao Paulo, Brazil.

[1]E. Wigner and F. Seitz, Phys. Rev. 43, 804 (1933).
[2]J. C. Slater, Phys. Rev. 45, 794 (1934).
[3]G. E. Kimball, J. Chem. Phys. 3, 560 (1935).
[4]F. Hund and B. Mrowka, Ber. Verh. Sächs. Akad. Wiss. Leipz. Math.-Phys. Kl. 87, 185 (1935).
[5]V. Zehler, Ann. Phys. (Leipz.) 13, 229 (1953).
[6]J. F. Mullaney, Phys. Rev. 66, 326 (1944).
[7]D. K. Holmes, Phys. Rev. 87, 782 (1952).
[8]E. Yamaka and T. Sugita, Phys. Rev. 90, 992 (1953).
[9]D. G. Bell, R. Hensman, D. P. Jenkins, and L. Pincherle, Proc. Phys. Soc. Lond. A 67, 562 (1954); D. P. Jenkins, Proc. Phys. Soc. Lond. A 69, 548 (1956).
[10]F. C. von der Lage and H. A. Bethe, Phys. Rev. 71, 612 (1947).
[11]F. Herman, Phys. Rev. 88, 1210 (1952); 93, 1214 (1954).
[12]F. Herman, R. L. Kortum, and C. D. Kuglin, Int. J. Quantum Chem. 1S, 533 (1967).
[13]G. S. Buberman, Usp. Fiz. Nauk 103, 675 (1971) [Sov.-Phys. Usp. 14, 180 (1971)].
[14]W. Kohn, Phys. Rev. 87, 472 (1952).
[15]For a comprehensive and up-to-date review of the cellular method, see S. L. Altmann, in *Orbital Theories of Molecules and Solids*, edited by N. H. March (Clarendon, Oxford, England, 1974), p. 30. See also: S. L. Altmann, Proc. R. Soc. A 244, 141, 153 (1958); S. L. Altmann and N. V. Cohan, Proc. Phys. Soc. Lond. 62, 383 (1958); S. L. Altmann and C. J. Bradley, Proc. Phys. Soc. Lond. 86, 915 (1965).
[16]J. M. Ziman, Solid State Phys. 26, 1 (1971).
[17]W. E. Rudge (unpublished).
[18]W. Saslow, T. K. Bergstresser, and M. L. Cohen, Phys. Rev. Lett. 16, 354 (1966).
[19]L. R. Saravia and D. Brust, Phys. Rev. 170, 683 (1968).
[20]L. A. Hemstreet, Jr., C. Y. Fong, and M. L. Cohen, Phys. Rev. B 2, 2054 (1970).
[21]R. Keown, Phys. Rev. 150, 568 (1966).
[22]R. C. Chaney, C. C. Lin, and E. E. Lafon, Phys. Rev. B 3, 459 (1971).
[23]G. S. Painter, D. E. Ellis, and A. R. Lubinsky, Phys. Rev. B 4, 3610 (1971).
[24]A. R. Lubinsky, D. E. Ellis, and G. S. Painter, Phys. Rev. B 6, 3950 (1972).
[25]R. A. Roberts and W. C. Walker, Phys. Rev. 161, 730 (1967).
[26]C. D. Clark, P. J. Dean, and P. V. Harris, Proc. R. Soc. A 277, 312 (1964).
[27]P. J. Dean, E. C. Lighttowlers, and D. R. Wright, Phys. Rev. 140, A352 (1965).
[28]F. R. McFeely, S. P. Kowalczyk, L. Ley, R. G. Cavell, R. A. Pollak, and D. A. Shirley, Phys. Rev. B 9, 5268 (1974).
[29]J. Keller, J. Phys. C 4, L85 (1971); 4, 314 (1971).
[30]A. R. Williams and J. van W. Morgan, J. Phys. C 5, 1293 (1972); 7, 36 (1974).
[31]F. Herman and S. Skillman, *Atomic Structure Calculations* (Prentice-Hall, Englewood Cliffs, N. J., 1963).
[32]F. Herman and S. Skillman, *Proceedings of the International Conference on Semiconductor Physics, Prague, 1960* (Publishing House of the Czechoslovak Academy of Sciences, Prague, 1961), p. 20.

[33]F. Herman, R. L. Kortum, C. D. Kuglin, and R. A. Short, in *Quantum Theory of Atoms, Molecules, and the Solid State*, edited by P. O. Löwdin (Academic, New York, 1966), p. 381.

[34]F. Herman, R. L. Kortum, C. D. Kuglin, J. P. van Dyke, and S. Skillman, Methods Comput. Phys. 8, 193 (1968).

[35]F. Herman, R. L. Kortum, I. B. Ortenburger, and J. P. van Dyke, Aerospace Research Laboratories Report ARL 69-0080, 1969 (unpublished).

[36]G. G. Hall, Philos. Mag. 43, 338 (1952). For recent applications of Hall's energy-band model, see D. Weaire and M. F. Thorpe, in *Computational Methods for Large Molecules and Localized States in Solids*, edited by F. Herman, A. D. McLean, and R. K. Nesbet (Plenum, New York, 1973), p. 295; W. A. Harrison, Phys. Rev. B 8, 4487 (1973); W. A. Harrison and S. Ciraci, Phys. Rev. B 10, 1516 (1974). A generalized version of Hall's model which includes next-nearest as well as nearest-neighbor overlap is given by J. C. Slater and G. F. Koster, Phys. Rev. 94, 1498 (1954).

[37]B. R. Cooper, E. L. Kreiger, and B. Segall, Phys. Rev. B 4, 1734 (1971).

[38]A. B. Chen, B. Segall, B. R. Cooper, and E. L. Kreiger, Phys. Rev. B 9, 3207 (1974); A. B. Chen and B. Segall (unpublished).

[39]S. L. Altmann and A. P. Cracknell, Rev. Mod. Phys. 37, 19 (1965).

[40]S. L. Altmann and C. J. Bradley, Proc. Phys. Soc. Lond. 86, 915 (1965).

[41]R. N. Euwema and D. J. Stukel, Phys. Rev. B 1, 4692 (1970).

[42]A. Baldereschi, Phys. Rev. B 7, 5212 (1973).

[43]D. J. Chadi and M. L. Cohen, Phys. Rev. B 7, 692 (1973).

[44]J. D. Joannopoulos and M. L. Cohen, J. Phys. C 6, 1572 (1973).

[45]J. C. Phillips, Comments Solid State Phys. 5, 113 (1973).

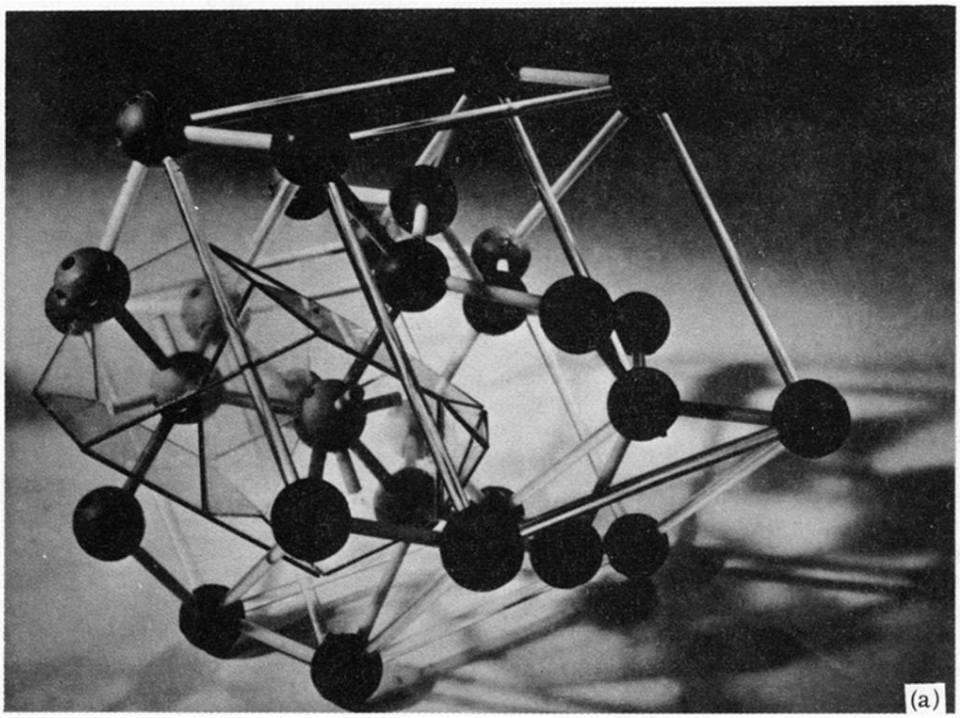

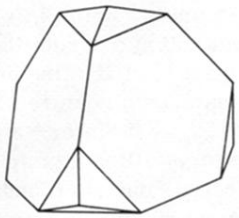

FIG. 2. (a) Model of diamond lattice showing the two Wigner-Seitz atomic polyhedra which together form the unit cell. All the hexagonal faces and only a few of the triangular faces of the atomic polyhedra are shown. The transparent rods indicate two interpenetrating unit cubes. The unit cube edge is a_L. (b) Atomic polyhedron for diamond structure (two-fold partitioning of unit cell).